Available online at www.sciencedirect.com
SCIENCE DIRECT®
Engineering Structures 25 (2003) 1019–1031
ENGINEERING STRUCTURES
www.elsevier.com/locate/engstruct

Comparison of measured and predicted response of manufactured circular steel tubular members under concentric and eccentric compressive and tensile loads

D.G. Linzell [a,*], A. Zureick [b], R.T. Leon [b]

[a] *Department of Civil and Environmental Engineering, State College, PA 16802, USA*
[b] *School of Civil and Environmental Engineering, The Georgia Institute of Technology, Atlanta, GA, 30332, USA*

Received 3 September 2002; received in revised form 5 February 2003; accepted 6 February 2003

Abstract

Tubular steel members are seeing increased usage both in building and bridge structures due to their efficient geometry and to aesthetic benefits that they offer over more traditional open, thin-walled cross sections. While the utilization of small (152 mm or less), stocky (wall thickness greater than 1.6 mm) diameter circular tubes has been increasing, experimental studies of these types of structural members have been rather limited, with most research focusing on large diameter, thin-walled tubes prevalent in offshore structures. Therefore, this manuscript discusses a series of tests of manufactured steel circular tubes under concentric and eccentric axial loads. These tests were performed to (1) examine their behavior, (2) develop instrumentation schemes and (3) ascertain the capacity of round tubular members used in cross-frames of a prototype curved steel bridge tested by the Federal Highway Administration as part of their Curved Steel Bridge Research Project. Testing procedures are described and results are presented and discussed. In addition, data produced from the tests was utilized to perform comparisons between experimental results and predicted capacities from AASHTO and AISC design specifications, which utilize approximations coupled with interaction concepts to quantify behavior. Results from the comparisons indicated that measured ultimate loads were an average of 1.3 times higher than values from factored AASHTO and AISC ultimate load predictions. However, when reduction factors were removed from the AASHTO or AISC prediction equations, actual ultimate loads were an average of 5% higher than predicted values, with certain predictions being slightly nonconservative. While the nonconservative predictions were attributed to member imperfections and slight specimen misalignment, they do demonstrate the sensitivity that can exist when attempting to predict stockier circular tube ultimate loads using approximate, design-based criteria.

Keywords: Manufactured; Steel; Circular; Tube; Eccentric; Concentric; Compressive; Tensile; Load experiment; Testing; Ultimate; Load

1. Introduction

Manufactured, or hot-formed seamless, steel circular tubes are increasingly used as both primary and secondary load carrying members in buildings and bridges. While extensive testing of large diameter and relatively thin-walled tubular members has occurred for offshore structures [1,2], limited published experimental data is available for circular steel tubes with outer diameters of 152 mm (6”) or less and wall thicknesses greater than 1.6 mm (1/16”). Results from a series of tests of such tubes are presented herein. The tubes were examined as part of a series of component studies from a large-scale curved three-girder bridge system tested by the Federal Highway Administration [3–6]. Extensively instrumented round tubular members were used in the cross-frames of the bridge system to monitor force redistribution that occurred as the curved girders buckled and yielded (Fig. 1). Tubular members were selected for the experimental bridge system over more standard angles and tee shaped cross-frame members to provide increased torsional stiffness and to help with instrumentation placement and data reduction.

* Corresponding author. Tel.: +1-814-863-8609; Fax: +1-814-863-7304.
E-mail address: dlinzell@engr.psu.edu (D.G. Linzell).

0141-0296/03/$ - see front matter © 2003 Elsevier Science Ltd. All rights reserved.
doi:10.1016/S0141-0296(03)00046-4

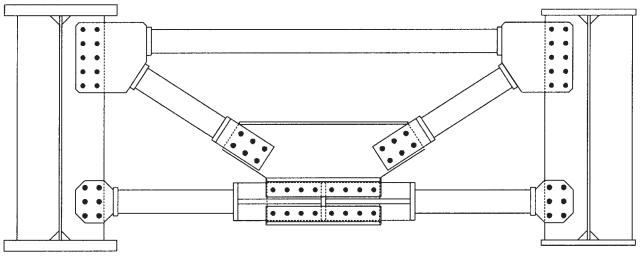

Fig. 1. Elevation of typical cross-frame (not to scale).

A number of experimental investigations of circular steel tubes have been conducted in the past. Such studies have generally been performed for the offshore structures industry, where circular cross-sections are extensively used. Full-scale and scale model circular tubes have been tested under a variety of loading and support conditions [7–16]. A summary of many of these tests is given by Prion and Birkemoe [2]. Another extensive series of tubular member tests was completed by CIDECT [17], although extensive details on the tests are unavailable. The tests described herein add to this existing database through the examination of stockier, small diameter steel tubes under combined axial and flexural loads and permit further verification of the accuracy of the current design equations for circular tubes given by the AASHTO Standard Specifications for Highway Bridges [18], the AISC Load and Resistance Factor Design Specification for Steel Hollow Structural Sections [17] and the AASHTO LRFD Bridge Design Specification [19]. Similar verification summaries of existing design equations have been performed in the past by Sherman [20] for both square and circular tubular members, however AASHTO criteria was not investigated. It should be noted that the research described herein focused purely on these design equations, which in certain cases involved simplifying and conservative approximations, and did not examine the accuracy of more accurate theoretical formulations that asses the capacity of tubular members under concentrically or eccentrically applied axial loads.

2. Objectives

A series of tests of manufactured circular steel tubes were completed:

1. to study behavior and ascertain ultimate capacity under a concentric and eccentric axial loads with pinned-pinned support conditions;
2. to develop schemes to determine axial force and bending moments in tubular members using minimal instrumentation; and
3. to examine and assess the accuracy of current AISC and AASHTO compression and tension member and beam-column design strength equations for circular tubes.

Items (1) and (3) will be discussed herein. Detailed discussions of Item (2) can be found elsewhere [4,6].

3. Experimental program

3.1. Test specimens

Tests of top chord and diagonal cross-frame members subjected to concentric and eccentric compressive and tensile loads were performed. All tests were carried out on manufactured, as opposed to fabricated, tubes. The tubes conformed to ASTM A513 Drawn Over Mandrel steel tube specifications with nominal yield strengths of 448 MPa (65 ksi). The tests were carried out on the longest and shortest members in any given cross-frame (i.e. top chord and diagonals in Fig. 1). Thirteen tests were performed with top chord specimens being examined under concentric and eccentric compressive and tensile loads and diagonal specimens being tested under concentric compressive loads. Nine of the top chord compression and tensile tests are discussed in detail herein.

Top chord specimens had nominal diameter to thickness ratios (D/t) of 20 (6.3 mm, 1/4” thick tubes) or 40 (3.2 mm, 1/8” thick tubes) using the full wall thickness (D/t ratios of 21.5 and 43.0 were obtained using 0.93t as specified in AISC HSS Specification 1.2), slenderness ratios (L/r) of 43, where L represented the tube length, and length to diameter (L/D) ratios of 15. Typical top chord compression specimens, indicating relevant geometric parameters, are shown in Fig. 2. Geometric properties for seven of the compression specimens (C1

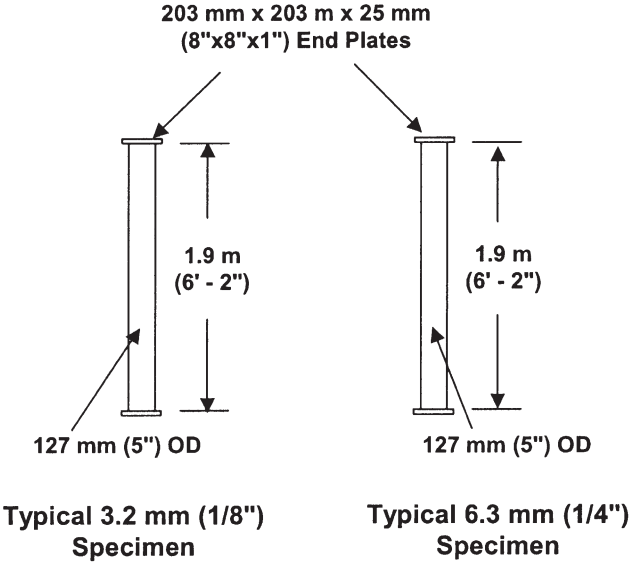

Fig. 2. Typical top chord compression specimen (not to scale).

Table 1
Geometric properties

Test	Concentric (C), eccentric (E)	Eccentricity mm (in)	Specimen length m (ft)	Specimen thickness mm (in)	Specimen diameter mm (in)	D/t	L/r	L/D
C1	C	–	1.9 (6.2)	3.17 (0.13)	127 (5.0)	39	43	15
C2	C	–						
C3	E	50.8 (2.0)						
C4	C	–		6.35 (0.26)		19	44	
C5	E	50.8 (2.0)						
C6	E	25.4 (1.0)						
C7	E	25.4 (1.0)						
T1	C	–						
T2	E	38.1 (1.5)						

to C7) and the two tensile specimens (T1 and T2) are summarized in Table 1. Geometry measurements for C1 to C3 (3.2 mm nominal thickness) were taken from samples from unyielded portions of actual specimens. Those for specimens C4 to C7, T1 and T2 (6.3 mm nominal thickness) were taken from a sampling of actual cross-frame members used in the experimental bridge. Specimens that were tested were from the same lot of materials.

Specimen material properties are summarized in Table 2. Material properties supplied from the manufacturer were verified using stub columns tests. Stub column tests were selected because their size gave a reasonable representation of residual stress distributions in the full-scale specimens. The tests were performed following procedures outlined in SSRC Technical Memorandum No. 3 of the Guide to Stability Design Criteria for Metal Structures [21]. Three tests were completed, two on 3.2 mm (1/8”) thick specimens and one on a 6.3 mm (1/4”) specimen. Comparisons between yield stresses from the manufacturer’s reports and the stub column tests showed good agreement with differences at or below 5%. Stub column yield stress magnitudes were slightly larger for the 3.2 mm (1/8”) specimens and slightly smaller for the 6.3 mm (1/4”) specimen. Yield stresses for all three stub column specimens were higher than the nominal value, which was 448 MPa (65 ksi).

3.2. Instrumentation and testing procedure

Specimen tests were conducted in a Riehle universal testing machine, with a capacity of 1800 kN (400 kips). The tubular sections were instrumented to monitor load, strain, displacement and rotation as shown in Fig. 3. Applied loads were measured using a 900 kN (200 kip) load cell affixed to the loading head of the universal testing machine. Transverse displacements were measured with potentiometers and LVDTs. The top of each specimen was instrumented with an inclinometer measuring rotation and a LVDT measuring transverse displacement to monitor any tendency of the loading to become a follower force. For the eccentric load tests, transverse displacements and end rotations were measured in the plane of bending. Data was acquired at half or one second intervals. Summaries of instrumentation used for each of the tests detailed herein are given in Table 3.

Fig. 3 details mid-height strain gage instrumentation used for the first two compression tests, C1 and C2. As Table 3 indicates, this instrumentation was representative of that used at mid-height for all six tests. Eight foil strain gages, alternating between single-arm gages and rosettes, were placed at 45° increments around the circumference of the tube. Rosettes were aligned so that their center arms fell on the longitudinal axis while sin-

Table 2
Material properties

Source	Thickness mm (in)	Prop. limit stress MPa (ksi)	Yield stress MPa (ksi)	Modulus of elasticity GPa (ksi)	Strain hardening modulus GPa (ksi)
Manufactuer cert. reports	3.175 (0.125)[a]	–	492 (72)	–	–
Manufactuer cert. reports	6.350 (0.250)[a]	–	582 (85)	–	–
Stub column test 1	3.251 (0.128)[b]	323 (47)	510 (74)	207 (30 000)	505 (800)
Stub column test 2	3.276 (0.129)[b]	317 (46)	503 (73)	207 (30 000)	4.8 (700)
Stub column test 3	6.426 (0.253)[b]	413 (60)	551 (80)	202 (29 268)	505 (800)

[a] Nominal.
[b] Measured.

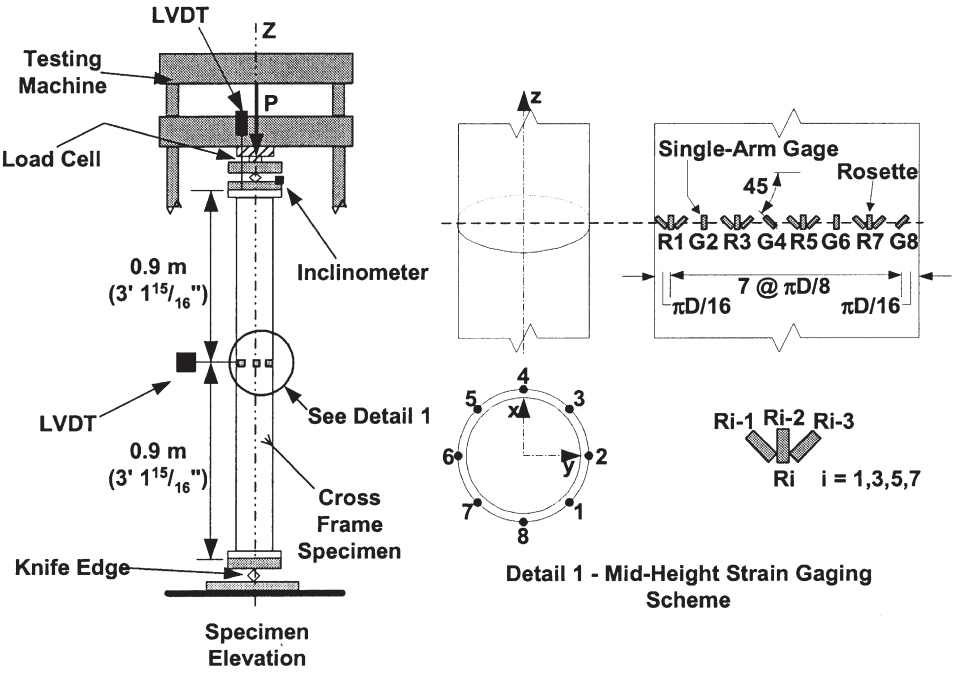

Fig. 3. C1, C2 elevation and details.

Table 3
Instrumentation summary, tests C1 to C7, T1 and T2

Test	Instrumentation			
	Load	Strain	Displacement	Rotation
C1, C2	Load cell at top	4 single-arm strain gages, 4 rosettes at mid-height	LVDT at mid-height, LVDT at top	Inclinom. at top
C3			LVDT at mid-height, potentiometer at mid-height, LVDT at top	
C4				
C5			2 potentiometers at mid-height, LVDT at top	
C6				
C7		4 single-arm strain gages, 4 rosettes at mid-height; 4 single-arm strain gages at 1/4∗L and 1.5∗D from ends	2 potentiometers at mid-height, potentiometers at 1/4∗L from ends, potentiometer on loading machine head, LVDT at top	
T1		4 single-arm strain gages, 4 rosettes at mid-height	LVDT at mid-height, potentiometer at mid-height, LVDT at bottom	Inclinom. at bottom
T2				

gle-arm gages were placed at alternating 0° and 45° angles with this axis.

At the beginning of each test a series of small loading cycles were applied to ensure that the specimens were correctly aligned. After alignment was achieved the tests were performed. The number of test loading cycles differed depending upon what was being studied and the type of investigation being performed (compression, tension, concentric, eccentric). Table 4 presents load history plots for specimens C1 to C7, T1 and T2.

4. Test descriptions and results

Specimens C1 to C7 were examined under compressive loads applied at different eccentricities from the specimen's longitudinal axis. They were supported top and bottom using hardened steel knife-edges that simulated pinned-pinned end conditions. Specimens T1 and T2 were studied under tensile loads applied concentrically and eccentrically using pins at their ends. Brief descriptions of each of these tests along with summaries

Table 4
Load histories, specimens C1 to C6

Test	Load history
C1, C2	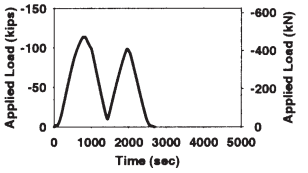
C3	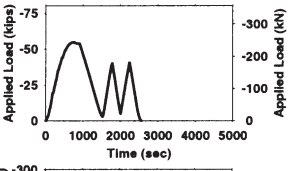
C4	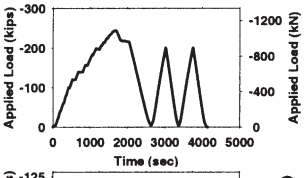
C5	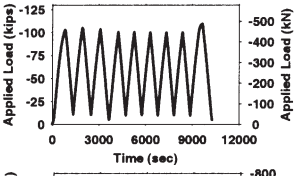
C6	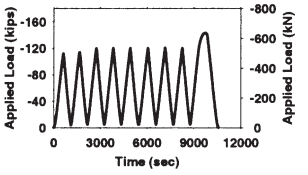
C7	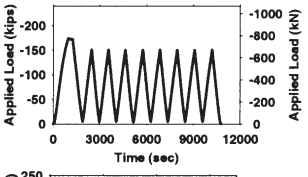
T1	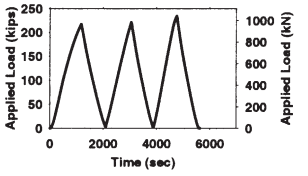
T2	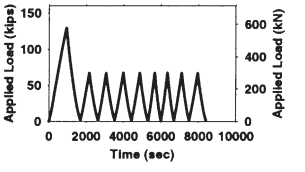

of experimental results are provided below. It should be noted that for all tests, minimal cross-sectional distortions and local buckling effects were observed at failure.

4.1. Specimens C1 and C2

A schematic of the testing configuration for C1 and C2, which had D/t ratios of 40 based on the full nominal thickness, is shown in Fig. 3. The specimens were identical except that end plates were attached to C1 using groove welds and to C2 using fillet welds (Fig. 2).

The variation in longitudinal mid-height strains with applied compressive force for C1 is shown in Fig. 4. The constant slope in the elastic region indicates that concentric loading was achieved. The maximum load was 556 kN (125.5 kips). Proportional limits were estimated using methods outlined for stub columns in SSRC Technical Memorandum No. 3 [21], which defines the proportional limit as the load when a 0.01 percent offset from the average longitudinal strain occurs. Specimen C1 reached its proportional limit at approximately 400 kN (90.0 kips).

Fig. 5 compares average calculated internal axial forces determined from either (a) the four rosettes or (b) the two single-arm gages aligned with the specimen's longitudinal axis (Fig. 3) to the applied axial force. A modulus of 200 GPa (29 000 ksi) and nominal cross-sectional areas were used in these calculations. P_{strain} represents axial forces determine using strain gage inputs while P_{appl} represents applied axial forces measured using the load cell. Convergence to P_{strain}/P_{appl} ratios near 1.0 in the elastic range would indicate that the strain gages could be used reliably to predict axial loads. Fig. 5 shows that both curves indicate an average ratio for P_{strain}/P_{appl} of 0.90 for the 400 measurements taken between 22 and 401 kN (5 and 90 kips) when the nominal thickness was replaced with 0.93t as recommended by the AISC HSS Specification. The ratio for P_{strain}/P_{appl} improved to 0.96 over this range when the full nominal thickness was used in the capacity calculations. When P_{strain}/P_{appl} was recalculated using measured geometric properties utilizing the full measured thickness, the ratio converged to 1.0. The results show, in general, very good agreement between measured loads from the load cell and forces computed from the strain gages when either full nominal or measured wall thicknesses were used.

Results for C2 did not differ appreciably from those obtained for C1. Specimen proportional limits and estimated ultimate loads were similar to those shown in Fig. 4 and the ratio of P_{strain}/P_{appl} was 0.95 when nominal geometric properties were used with the full nominal thickness instead of 0.93t. Values converged to 0.87 when 0.93t was used instead of the full nominal thickness and to 0.97 when the full measured thickness was used.

4.2. Specimen C3

Set-up and instrumentation was similar to that shown in Fig. 3 for C1 and C2 with a 50.8 mm (2") load eccentricity imposed by shifting the specimens relative to the line-of-action of the testing machine's applied load. Specimen C3 was tested to help establish capacity limits for 3.2 mm (1/8") thick top chord specimens with nomi-

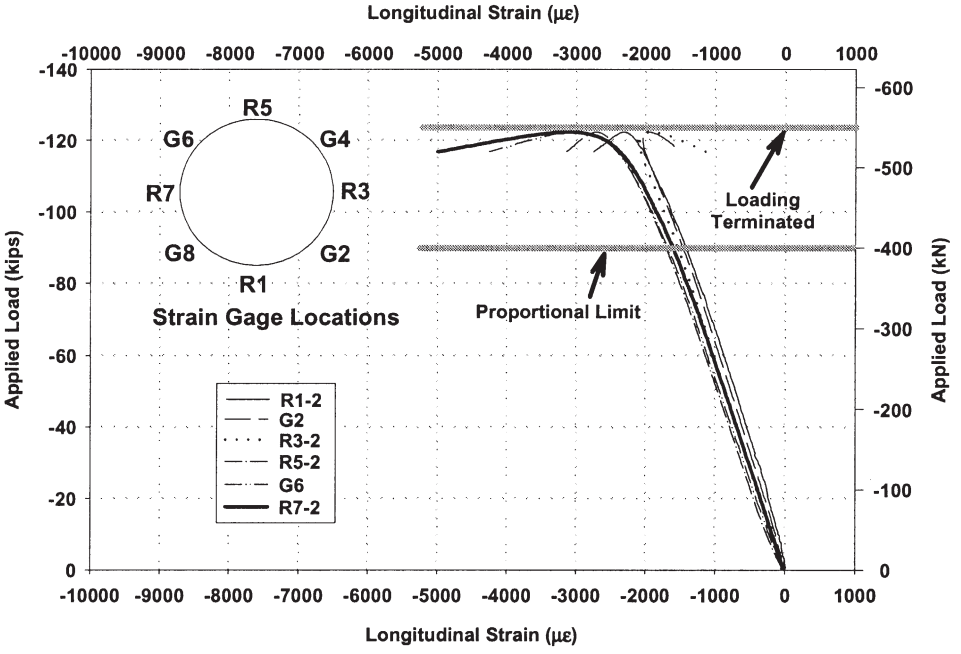

Fig. 4. Applied load vs. longitudinal strain, first loading cycle, specimen C1.

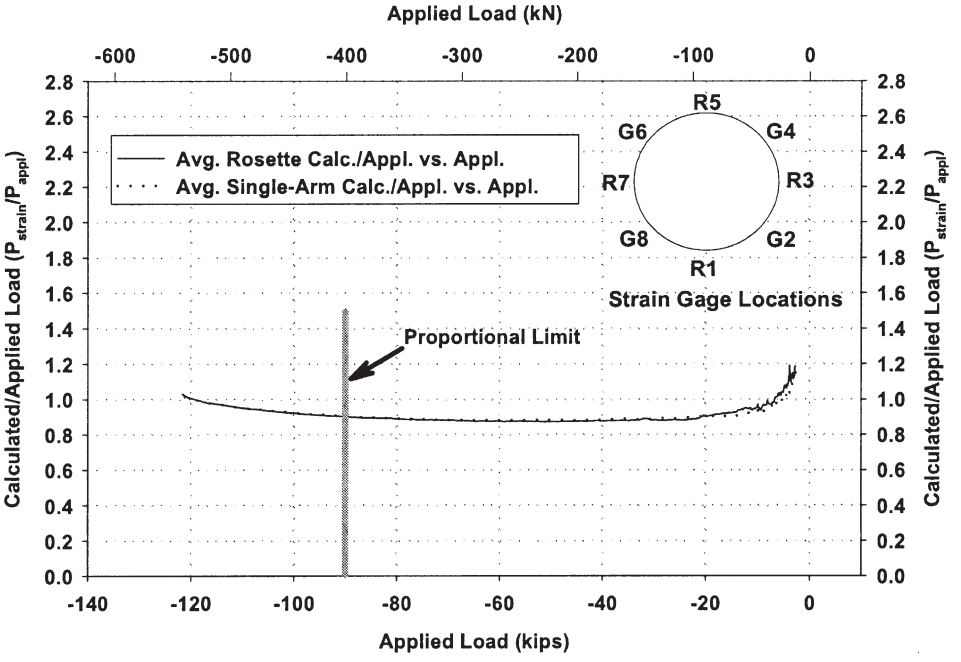

Fig. 5. Average calculated/applied load ratios, first loading cycle, specimen C1.

nal D/t ratios of 40 under combined axial and flexural effects.

The proportional limit was reached at an applied load of 178 kN (40 kips) with an ultimate load of 267 kN (60 kips). Fig. 6 shows that P_{strain}/P_{appl} ratios averaged 0.91 when nominal geometric properties were used with the full thickness. Values converged to 0.84 when 0.93t was used to calculate P_{strain} and to 0.94 with the measured thickness. Fig. 7 examines the accuracy of calculated (internal) moments determined using the strain gages through comparisons to applied (external) moments determined using applied loads and mid-height lateral displacement data. Again, ratios converged to 0.91 in the elastic range when nominal geometric properties were used with the full thickness, to 0.84 when 0.93t was used, and to 0.93 when using the measured wall thickness.

When experimental results for specimens C1 to C3

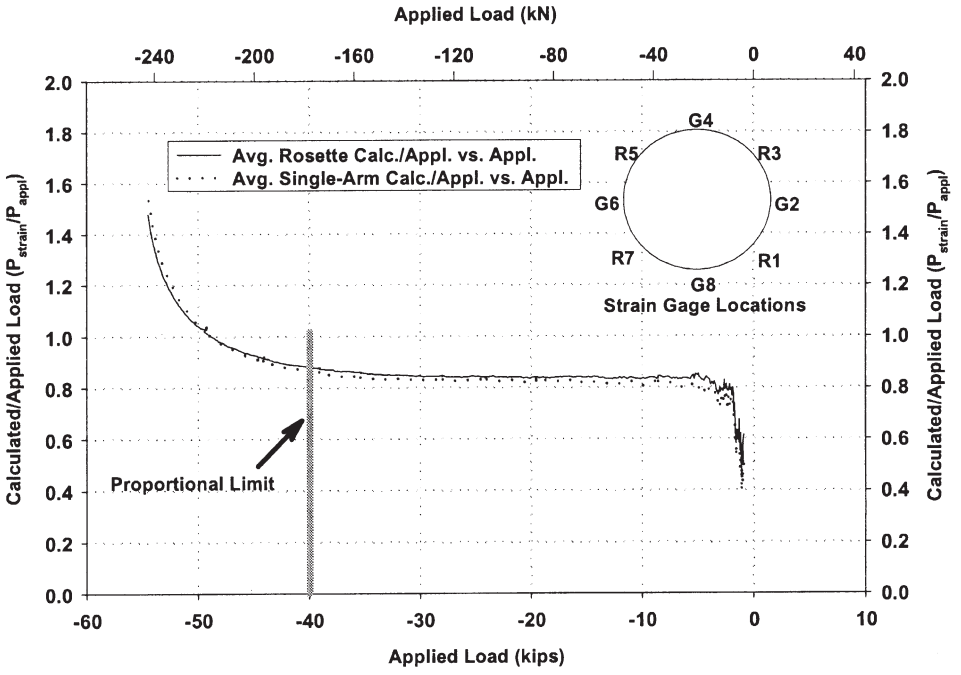

Fig. 6. Average applied/calculated load ratios vs. applied load, first loading cycle, specimen C3.

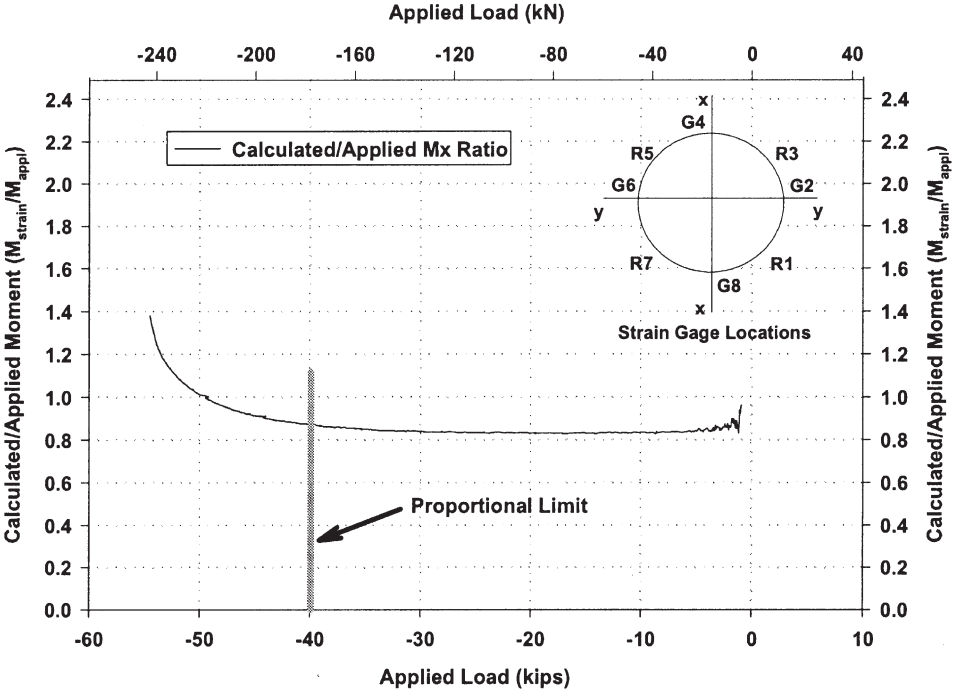

Fig. 7. Calculated/applied moment ratios (Mx) vs. applied load, first loading cycle, specimen C3.

were compared to predicted cross-frame member loads in the experimental curved bridge, they indicated that an increase in wall thickness would be required to prevent premature yielding. Therefore, additional tests were deemed necessary and specimens C4 to C7, which had wall thicknesses of 6.3 mm (1/4”), were fabricated and tested.

4.3. Specimen C4

Specimen C4 examined the behavior of a 6.3 mm (1/4”) specimen, nominal $D/t = 20$, under concentric compressive loads. The testing configuration and instrumentation were identical to that for C1 and C2 (Fig. 3) and the load history was similar to that for C3 (Table

4). The proportional limit load occurred at 979 kN (221 kips) with an ultimate load approaching 1112 kN (250 kips). These values are nearly double those for the 3.2 mm (1/8") thick specimens C1 and C2. As was shown for C1 to C3, internal axial force estimates from the single-arm strain gages and rosettes were within 10% of actual values when either the full nominal thickness or the measured thickness were used.

4.4. Specimens C5 and C6

Specimens C5 and C6 examined 6.3 mm (1/4") specimens (nominal D/t = 40) with imposed loads at 50.8 mm (2") and 25.4 mm (1") eccentricities, respectively. The tests were completed to establish capacity limits for 6.3 mm (1/4") top chord specimens under combined axial and flexural effects. They also provided further verification of equations used to determine internal axial loads and bending moments. After being properly aligned in the testing machine, both tests involved a total of nine loading cycles, eight to the proportional limit and one to ultimate. Their load histories are summarized in Table 4.

Results from test C5 indicated a proportional limit of approximately 356 kN (80 kips), which again was nearly double the value for the 3.2 mm (1/8") thick specimen examined at a similar eccentricity for test C3 (Table 1). The specimen's ultimate load was 534 kN (120 kips). C6 indicated yielding at 534 kN (120 kips) with an ultimate load of 667 kN (150 kips). Comparisons between internal and external axial loads and moments for both specimens C5 and C6 again showed good agreement when full nominal or measured wall thickness values were used.

4.5. Specimen C7

C7 examined the behavior of a 6.3 mm (1/4") top chord specimen in double curvature by shifting the knife-edges at the ends in opposite directions relative to the specimen's longitudinal axis (Fig. 8). Eccentricities were 25.4 mm (1"). Horizontal shears that developed during C7 testing caused lateral displacement of the testing machine top loading head. The effect of this translation was removed during post-processing of the data, using a correction based on the horizontal displacement of the top of the loading machine. Comparisons between strain readings at mid-height, at the quarter points and at 1.5 times the diameter from the ends for C7 indicated that, while the knife-edges permitted rotation, they provided a certain amount of fixity at the ends. Examination of the experimental data indicated a proportional limit at an applied compressive load of 623 kN (140 kips). Good agreement was shown between applied and predicted axial loads when full nominal or measured wall thickenesses were used. However, lateral translations that occurred influenced comparisons between calculated and applied moments so that no clear conclusions could be made. In addition, no clear estimation of an ultimate load could be obtained from the experimental data.

4.6. Specimens T1 and T2

Two tensile tests of cross-frame top chord specimens were performed to assess the validity of proposed instrumentation schemes for cross-frame members under tensile loads. Test T1 examined the behavior of a 6.3 mm (1/4") thick top chord specimen under concentric tensile loads. As indicated in Fig. 9, connections between the specimen and the testing machine were achieved using pins inserted through vertical plates at each end. Test T2 examined the behavior of a similar top chord specimen under an eccentrically applied tensile load. Load eccentricity was obtained using the same testing apparatus for test T1 by shifting the specimen 38.1 mm (1.5") along the pins. A series of elastic cycles were used to align each specimen in the testing machine prior to the tests (Table 4). Experimental proportional limits were 712 kN (160 kips) and 445 kN (100 kips) for T1 and T2, respectively. Experimental ultimate loads were not obtained for either test. As was demonstrated for the majority of the compression tests, good agreement between applied and calculated axial forces and moments was demonstrated when full nominal or measured wall thickness values were used.

5. Comparisons to AISC and AASHTO predictions

Predicted ultimate axial loads for each compression specimen were determined using equations given in: (1) the AASHTO Standard Specifications for Highway Bridges [18]; (2) AISC Load and Resistance Factor Design Specification for Steel Hollow Structural Sections [17]; and (3) the AASHTO LRFD Bridge Design Specifications [19]. The presented concentrically loaded specimen capacity equations in all three specifications were obtained from fundamental stability theory accounting for global and local buckling and modified to account for geometric and material imperfections and unintended load eccentricities. Eccentric specimen equations from all three specifications utilize interaction principles coupled with conservative assumptions to ensure that member capacities are not exceeded due to combined axial and flexural effects and any secondary effects resulting from deformations occurring along the member length. For the current study, concentric specimen ultimate loads were found directly from equations given in the specifications, while eccentric specimen loads were found from modified versions of interaction equations rewritten to solve for axial loads at a given eccentricity.

AASHTO Standard Specification equations were

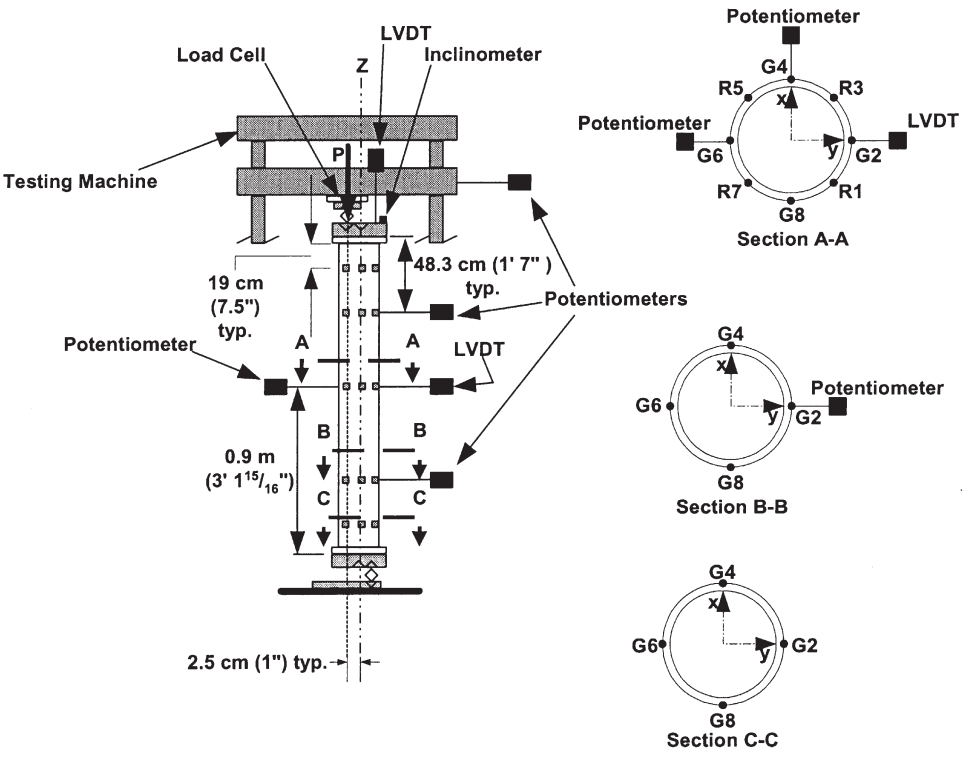

Fig. 8. C7 elevation and details (not to scale).

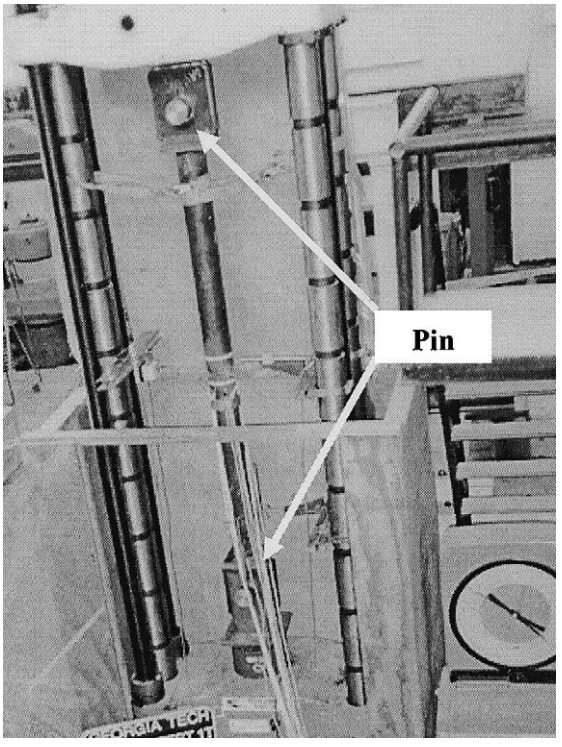

Fig. 9. Specimen T1.

taken from Article 10.54. Concentrically loaded compression tests had their ultimate values compared to Eq. (10-150):

$$P_u = 0.85 A_s F_{cr} \tag{1}$$

where P_u, maximum axial force; A_s, cross-sectional area; $F_{cr} = F_y\left[1-\frac{F_y}{4\pi^2 E}\left(\frac{KL_c}{r}\right)^2\right]$; F_y, yield stress; E, Young's modulus; K, effective length factor; L_c, length between support points; r, radius of gyration.

Experimental ultimate axial loads from the eccentric compressive tests were compared to modified equations from Article 10.54.2 of the AASHTO Standard Specification. Two interaction equations are provided, (10-155) and (10-156), to evaluate the behavior of a member under combined axial load and bending:

$$\frac{P}{0.85 A_s F_{cr}} + \frac{MC}{M_u\left(1-\frac{P}{A_s F_e}\right)} \le 1.0 \tag{2}$$

$$\frac{P}{0.85 A_s F_y} + \frac{M}{M_p} \le 1.0 \tag{3}$$

where P, maximum axial force; M, maximum bending moment; C, equivalent moment factor = 1.0; M_u, ultimate bending strength = $F_y Z$; Z, plastic modulus =

1.7∗S; S, section modulus; $F_e = \frac{E\pi^2}{\left(\frac{KL_c}{r}\right)^2}$; M_p, plastic moment = M_u.

The remaining variables have been previously defined.

For eccentrically loaded specimens, Eqs. (2) and (3) were each rearranged to solve for maximum axial loads by replacing M with P∗e. The solution to Eq. (2) appears as:

$$P \leq \left(\frac{1}{2M_u}\right)(A + B) \tag{4}$$

where

$$A = -M_u A_s F_e - 0.85 e A_s^2 F_{cr} F_e - 0.85 M_u A_s F_{cr} \tag{5}$$

and

$$B = \sqrt{M_u^2 A_s^2 F_e^2 + 2\cdot 0.85 M_u A_s^3 F_{cr} F_e^2 - 2\cdot 0.85 M_u^2 A_s^2 F_{cr} F_e + 0.85^2 e^2 A_s^4 F_{cr}^2 F_e^2 + 2\cdot 0.85^2 e M_u A_s^3 F_{cr}^2 F_e + 0.85^2 M_u^2 A_s^2 F_{cr}^2} \tag{6}$$

and Eq. (3) becomes:

$$P \leq \frac{1}{\frac{1}{0.85 A_s F_y} + \frac{e}{M_p}}. \tag{7}$$

The smallest value for P from Eq. (4) or (7) was said to be the ultimate load for that specimen.

Similar equations were obtained from the AISC and AASHTO Specifications. The AISC concentric compression equation is from Article 4.2 of the AISC HSS Specification and appears as:

$$P_u = \phi_c A_g F_{cr} \tag{8}$$

where P_u, maximum axial force; ϕ_c, resistance factor for compression = 0.85, A_g, cross sectional area; $F_{cr} = Q(0.658^{Q\lambda_c^2})F_y$; $\lambda_c = \frac{KL}{r\pi}\sqrt{\frac{F_y}{E}}$; Q, 1.0;L, unbraced length.

Remaining terms in Eq. (8) were as defined for Eqs. (2) to (7). The AISC eccentric compression equation was modified from Eq. 7.1-1 in the AISC HSS Specification and appears in its final form as:

$$P_u \leq \frac{F_y}{\left(\frac{1}{\phi_c A_g} + \frac{8e}{9\phi_b Z}\right)} \tag{9}$$

where ϕ_c, resistance factor for compression = 0.85; ϕ_b, resistance factor for bending = 0.9; Z, plastic modulus.

Remaining terms in Eq. (9) are similar to those found in Eq. (2) to (7).

The AASHTO LRFD concentric and eccentric compression equations are from Articles 6.9.2 and 6.9.4 of the specification and are identical to those shown above from AISC. The only differences between the AASHTO LRFD and AISC equations are the resistance factors that are used. AASHTO requires ϕ_c of 0.9 for tubes under concentric and eccentric compression and ϕ_b of 1.0 for tubes in flexure.

Ultimate strength calculations were performed for the compression tests discussed herein (C1 to C7) and results are presented in Tables 5 and 6. Experimentally obtained ultimate loads from the load cells (P_{exp}) are nondimensionalized with respect to the lowest predicted ultimate axial load from Eqs. (1) to (9). Table 5 contains results that include the resistance factors and use nominal tubular member yield stresses and cross-sectional dimensions. Pinned end conditions were assumed.

Table 6 contains unfactored AASHTO and AISC ultimate loads found using measured geometric and material properties. To obtain 'unfactored' values from the AASHTO Standard Specifications, the 0.85 reduction coefficient shown in those equations (see Eqs. (2) to (7)) was removed. For the 3.2 mm (1/8") thick specimens, the measured thickness was an average of measurements taken from the specimens that were tested. For the 6.3 mm (1/4") specimens, the measured thickness was averaged from a larger data set of measurements of cross-frame members used in the experimental bridge.

Predictions shown in Table 5 for the ultimate loads were conservative for all of the tests, as expected, with actual ultimate loads being generally 1.3 to 1.6 times higher than factored nominal predictions. There were generally minor differences in the level of conservatism between the AASHTO Standard Specification, AASHTO LRFD and AISC HSS equations although the AASHTO LRFD predictions were slightly less conservative (10% or less) than the other two specifications.

The unfactored AISC and AASHTO interaction equations provided conservative ultimate load predictions for the 3.2 mm (1/8") thick specimens, which were calculated using an average measured thickness taken from the specimens, and generally conservative predictions for the 6.3 mm (1/4") specimens, which utilized an average measured thickness taken from a sampling of members from the same lot of materials that was tested and used in the experimental curved bridge. The level of conservatism was reduced for both specimen thicknesses as load eccentricities were introduced and that predictions for the 6.3 mm (1/4") specimens were generally less conservative than those for the 3.2 mm (1/8") specimens. In fact, unfactored predictions for C6, the 6.3 mm (1/4") thick specimen tested at a 25.4 mm (1") eccentricity, were nonconservative for all specifications. It should be

Table 5
C1 to C11 ultimate axial loads, nominal geometric and material properties

Test	AASHTO slenderness ratio ($^{KL}/_{r}$)	AISC slenderness ratio ($^{KL}/_{r}$)	Experimental proportional limit load kN (kips)	Experimental ultimate load kN (kips)	Nondim. ratios - AASHTO std. spec. factored ultimate load (P_{exp}/P_{calc})	Nondim. ratios - AISC LRFD factored ultimate load (P_{exp}/P_{calc})	Nondim. ratios - AASHTO LRFD factored ultimate load (P_{exp}/P_{calc})
C1	39.1	44.7	400(90)	556(125)	1.4	1.5[b]	1.4[c]
C2	39.1	44.7	356 (80)	512 (115)	1.3[a]	1.4[b]	1.3[c]
C3	39.1	44.7	178 (40)	267 (60)	1.4[d]	1.3[e]	1.2[f]
C4	40.1	45.8	979 (220)	1112 (250)	1.4[a]	1.6[b]	1.5[c]
C5	40.1	45.8	356 (80)	534 (120)	1.5[d]	1.3[e]	1.2[f]
C6	40.1	45.8	534 (120)	667 (150)	1.4[d]	1.2[e]	1.1[f]
C7	40.1	45.8	623 (140)	–	–	–	–

[a] AASHTO Std. Spec. Eqn. 10-150.
[b] AISC HSS Article 4.2.
[c] AASHTO LRFD. Eqn. 6.9.2.1-1.
[d] AISC HSS Eqn. 7.1-1.
[e] AASHTO Std. Spec. Eqn. 10-155.
[f] AASHTO LRFD Eqn. 6.9.2.2-2.

Table 6
C1 to C11 ultimate axial loads, measured geometric and material properties

Test	AASHTO slenderness ratio ($^{KL}/_{r}$)	AISC slenderness ratio ($^{KL}/_{r}$)	Experimental proportional limit load kN (kips)	Experimental ultimate load kN (kips)	Nondim. ratios - AASHTO std. spec. factored ultimate load (P_{exp}/P_{calc})	Nondim. ratios - AISC LRFD factored ultimate load (P_{exp}/P_{calc})	Nondim. ratios - AASHTO LRFD factored ultimate load (P_{exp}/P_{calc})
C1	39.1	44.7	400 (90)	556 (125)	1.2[a]	1.3[b]	1.3[c]
C2	39.1	44.7	356 (80)	512 (115)	1.1[a]	1.2[b]	1.2[c]
C3	39.1	44.7	178 (40)	267 (60)	1.3[d]	1.1[e]	1.1[f]
C4	39.7	45.4	979 (220)	1112 (250)	0.9[a]	1.0[b]	1.0[c]
C5	39.7	45.4	356 (80)	534 (120)	1.0[d]	0.8[e]	0.8[f]
C6	39.7	45.4	534 (120)	667 (150)	0.9[d]	0.8[e]	0.8[f]
C7	39.7	45.4	623 (140)	–	–	–	–

[a] AASHTO Std. Spec. Eqn. 10-150.
[b] AISC HSS Article 4.2.
[c] AASHTO LRFD. Eqn. 6.9.2.1-1.
[d] AISC HSS Eqn. 7.1-1.
[e] AASHTO Std. Spec. Eqn. 10-155.
[f] AASHTO LRFD Eqn. 6.9.2.2-2.

noted that, when the AISS LRFD interaction equations were developed, a small level of nonconservatism was permitted [22].

While this lack of conservatism can be largely attributed to errors in the calculations from variations in wall thicknesses and/or diameters from average measured values along with slight misalignment of the specimens affecting the experimental results, it should be noted that amplification effects on the behavior were not incorporated into the determination of P_{calc}. Accounting for second-order geometric effects is discussed in the commentaries for AASHTO LRFD Article 9.2.2 and for AISC HSS Article 7.1. No such discussion is provided in the AASHTO Standard Specification criteria. Therefore, amplification effects were not incorporated into any of the calculations.

The effects of second-order behavior appear minimal, however, when, for example, the approximate procedure presented in Article C1.2 of the AISC LRFD Specification for Structural Steel Buildings [23] is used to amplify flexural behavior for C6. Eqs. C1-1 and C1-2 are applicable for amplifying the flexural effects that occur in the specimens that were tested, which did not have lateral translation. Those equations appear, when modified for the effect of no lateral translation, as:

$$M_u = B_1 M_{nt} \tag{10}$$

and

$$B_1 = \frac{C_m}{(1-P_u/P_{e1})} \geq 1 \quad (11)$$

where B_1, amplification factor; M_{nt}, member flexural strength assuming no lateral translation (sway); $C_m = 0.6-0.4\left(\frac{M_1}{M_2}\right)$; $\left(\frac{M_1}{M_2}\right)$, ratio of larger/smaller end moments; $P_{e1} = \frac{\pi^2 EI}{(KL)^2}$ and the remaining variables were previously defined. When Eq. (10) is used to approximate an amplification factor based upon the ultimate load obtained experimentally, the calculated factor is less than 1.0, which implies that negligible amplification occurs.

Experimental ultimate loads were not obtained for either of the tensile tests and ultimate load comparisons similar to those provided in Table 5 and Table 6 could not be performed.

6. Conclusions

The work summarized herein details a series of tests of manufactured circular steel tubes. The specimens were full-scale reproductions of cross-frame members from an experimental curved bridge tested by the Federal Highway Administration. They were examined individually to develop instrumentation schemes and to provide insight into the behavior of manufactured circular steel tubular members under a variety of loading scenarios. Conclusions drawn from the nine tests detailed herein include the following:

- Reliable measurements of internal axial forces and bending moments were obtained from strain gages mounted to the specimens.
- Acceptable levels of conservatism existed when axial loads were predicted using the full nominal thickness as opposed to a reduced thickness recommended by the AISC Load and Resistance Factor Design Specification for Steel Hollow Structural Sections (0.93t) for the range of specimens that were tested herein.
- Factored predictions for manufactured circular steel tube ultimate compressive loads using AASHTO or AISC design equations with nominal geometric and material properties were conservative, being on average 30% higher than the measured values.
- Of the three specifications, the AASHTO LRFD Bridge Design Specification provided the least conservative nominal ultimate load prediction, although the values were only slightly less (within 10%) than those obtained from the other two specifications.
- The level of conservatism of unfactored predictions for manufactured circular steel tube compressive ultimate loads using the AASHTO and AISC equations decreased, as was expected, to an average level of conservatism of around 5%.
- The effects of amplification on behavior were shown to be minimal for the compression specimens that were tested.
- Nonconservative ultimate load predictions were obtained for all of the 6.3 mm (1/4”) specimens that were tested and, while these values are of concern, they are attributed largely to two items unrelated to how the interaction equations were formulated: (1) differences in tested specimen wall thicknesses from measured values that were used, which, while being taken from similarly-sized specimens used in the experimental bridge to provide a larger data set, were not from specimens that were tested, and (2) unrecorded specimen imperfections influencing behavior.
- While the nonconservative results can be attributed to changes of testing variables and not to errors in equation formulation, the level of sensitivity exhibited by the presented equations for approximating ultimate loads for the range of specimens that were tested indicates that detailed information regarding member properties and imperfection levels need to be obtained if more accurate or slightly conservative ultimate load predictions are desired for stockier circular tubes utilizing interaction concepts.

Acknowledgements

This work was supported by HDR Engineering thrA under Contract No. DTFH61-92-C-00136. Sheila Duwadi serves as the Contracting Officer’s Technical Representative for FHWA. Technical input from Dann Hall and Mike Grubb of BSDI and the assistance of Bill Wright of FHWA was greatly appreciated.

References

[1] Sherman DR. Post local buckling behavior of tubular strut type beam-columns: an experimental study, Report to Shell Oil Co., University of Wisconsin-Milwaukee 1980.
[2] Prion HGL, Birkemoe PC. Beam-column behavior of fabricated steel tubular members. ASCE Jnl of Struct Eng 1992;118(5):1213–32.
[3] Duwadi SR, Yadlosky JM, Yoo CH. Horizontally curved steel bridge research—update 2. In: Proc 1994 ASCE Struct Cong. 1994. p. 1071–6.
[4] Linzell DG. Studies of a full-scale horizontally curved steel I-girder bridge system under self-weight. Ph.D. dissertion, School of Civil and Environmental Engineering, Georgia Institute of Technology, Atlanta 1999.
[5] Zureick A, Leon RT, Burrell J, Linzell D. Curved steel bridges—experimental and analytical studies. In: Proc Innovations in Struct Design: Strength, Stability, Reliability. A Symposium Honoring Theodore V. Galambos. SSRC. 1997. p. 179–90.
[6] Zureick A, Linzell D, Leon RT, Burrell J. Curved steel I-girder bridges - experimental and analytical studies. Eng Struct 2000;22(2):180–90.
[7] Schilling CG. Buckling strength of circular tubes. ASCE Jnl of the Struct Div 1965;91(ST5):325–48.

[8] Sherman DR. Tests of circular steel tubes in bending. ASCE Jnl of the Struct Div 1976;102(ST11):2181–95.
[9] Ostapenko O, Gunzelman SX. Local buckling of tubular steel columns. In: Proc of the National Struct Eng Conf. Methods of Structural Analysis. 1976. p. 549–68.
[10] Chen WF, Ross DA. Tests of fabricated tubular columns. ASCE Jnl of Struct Eng 1977;103(ST3):619–34.
[11] Marzullo MA, Ostapenko O. Tests on two high-strength short tubular columns. In: Proc of the 10th Annual Offshore Tech Conf. 1978. p. 327–34.
[12] Miller CD. Tension and collapse tests of fabricated steel cylinders. In: Proc. of the 14th Annual Offshore Tech. Conf. 1982. p. 634–41.
[13] Matsui C, Tsuda K. Strength and behavior of circular steel tubular beam columns. In: Proc Int'l Conf on Steel Struct. Recent Research Advances and Their Applications to Design. Yugoslavia: Civil Engineering Faculty, Belgrade University; 1986. p. 327–32.
[14] Miller CD. Summary of buckling tests on fabricat steel cylindrical shells in USA. In: Offshore structures III: Buckling of shells in offshore structures. 1982. p. 429–47.
[15] O'Shea MD, Bridge RQ. Local buckling of thin-walled circular steel sections with or without internal restraint. Jnl of Construct Steel Res 1997;41(2-3):137–57.
[16] Yang XM. Study of carrying capacity of fabricated tubular columns under axial compression. In: Proc. of the Annual Tech. Session, SSRC. Washington, DC: AISI; 1987.
[17] American Institute of Steel Construction. Load and resistance factor design specification for steel hollow structural sections. Chicago IL, 2000.
[18] American Association of State Highway and Transportation Officials. Standard specifications for highway bridges, 16th ed. Washington DC, 1996.
[19] American Association of State Highway and Transportation Officials. LRFD bridge design specification, 2nd ed. Washington DC, 1998.
[20] Sherman DR. Impact of code difference for tubular members. Jnl. of Construct Steel Res 1991;18:317–25.
[21] Galambos TV, editor. Guide to stability design criteria for metal structures, 5th edn. SSRC; 1998.
[22] Salmon CG, Johnson JE. Steel structures, design and behavior, 4th edn. New York: Harper-Collins, 1996.
[23] American Institute of Steel Construction. Load and resistance factor design specification for structural steel buildings. Chicago, IL, 2000.